Laminated Ultrathin Chemical Vapor Deposition Graphene Films Based Stretchable and Transparent High-Rate Supercapacitor

Ping Xu,[†,‡] Junmo Kang,[§] Jae-Boong Choi,[§,∥] Jonghwan Suhr,[⊥] Jianyong Yu,[†,*] Faxue Li,[†] Joon-Hyung Byun,[#] Byung-Sun Kim,[#] and Tsu-Wei Chou[‡,*]

[†]College of Textiles, Donghua University, Shanghai 201620, People's Republic of China, [‡]Department of Mechanical Engineering, University of Delaware, Newark, Delaware 19716, United States, [§]SKKU Advanced Institute of Nanotechnology (SAINT) and Center for Human Interface Nano Technology (HINT), [∥]School of Mechanical Engineering, and [⊥]Department of Polymer Science and Engineering, Department of Energy Science, Sungkyunkwan University, 440-746 Suwon, South Korea, and [#]Composites Research Center, Korean Institute of Materials Science, Changwon 641831, South Korea

ABSTRACT Due to their exceptional flexibility and transparency, CVD graphene films have been regarded as an ideal replacement of indium tin oxide for transparent electrodes, especially in applications where electronic devices may be subjected to large tensile strain. However, the search for a desirable combination of stretchability and electrochemical performance of such devices remains a huge challenge. Here, we demonstrate the implementation of a laminated ultrathin CVD graphene film as a stretchable and transparent electrode for supercapacitors. Transferred and buckled on PDMS substrates by a prestrainingi-then-buckling strategy, the four-layer graphene film maintained its outstanding quality, as evidenced by Raman spectra. Optical transmittance of up to 72.9% at a wavelength of 550 nm and stretchability of 40% were achieved. As the tensile strain increased up to 40%, the specific capacitance showed no degradation and even increased slightly. Furthermore, the supercapacitor demonstrated excellent frequency capability with small time constants under stretching.

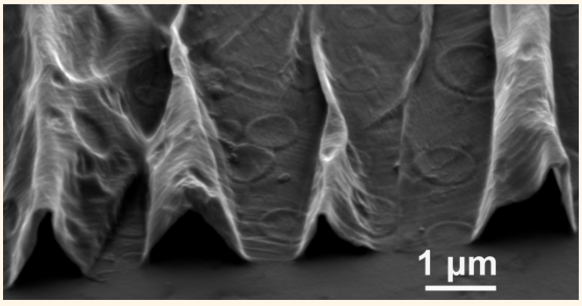

KEYWORDS: chemical vapor deposition · graphene films · stretchability · transparency · high rate capability · supercapacitors

Graphene, a 2D monatomic layer with sp^2-hybridized carbon atoms arranged in a hexagonal configuration, possesses extraordinary properties, such as strong mechanical strength, superb flexibility, excellent electrical conductivity, large specific surface area, high optical transparency, and good chemical stability.[1−4] It has demonstrated an enormous potential in a variety of fields, encompassing nanocomposites, optoelectronic devices, sensors, actuators, microelectronics, and energy storage devices.[5,6] Numerous approaches for graphene synthesis have been developed; these include mechanical exfoliation (the Scotch tape and AFM method), epitaxial growth on silicon carbide, chemical vapor deposition (CVD), reduction from chemically exfoliated graphene oxide, unzipping carbon nanotubes, and so forth. Among them, reduction from chemically exfoliated graphene oxide has been the most prevailing, low-cost, and scalable process. Unfortunately, the as-received graphene suffers from poor electrical conductivity owing to poor interlayer junction contacts, structural defects, and incomplete reduction caused by vigorous exfoliation and reduction processes.[4,5] Therefore, chemical vapor deposition, which can synthesize large-area graphene film on inexpensive Ni and Cu foils, has emerged as a desirable approach. Particularly, when compared to the nonuniform multilayer graphene obtained on Ni substrates, predominantly monolayer graphene of high quality produced on polycrystalline Cu foil is more favorable for applications as electrodes of supercapacitors where high conductivity is essential.[3,7−9]

A review of the substantial amount of literature on graphene-based supercapacitors reveals that there are very few reports on the electrochemical performance of CVD

* Address correspondence to yujy@dhu.edu.cn; chou@udel.edu.

Received for review July 1, 2014 and accepted August 21, 2014.

Published online August 21, 2014
10.1021/nn503570j

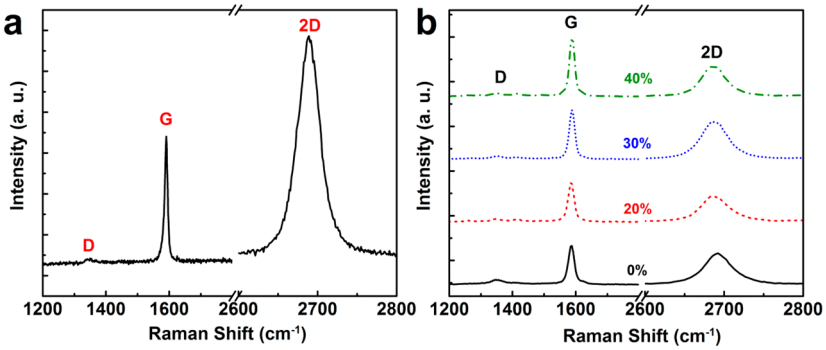

Figure 1. Raman spectra of graphene films. (a) Raman spectrum of as-received monolayer graphene film on SiO_2/Si substrate. (b) Raman spectrum variation of a four-layer buckled graphene/PDMS film with the tensile strain.

graphene films. The supercapacitor based on vertically oriented graphene nanosheets that were synthesized using radio frequency plasma-enhanced CVD was reported to be able to efficiently filter 120 Hz current.[10,11] One to two layers of CVD graphene were first fabricated into ultrathin supercapacitors using an "in-plane" method with a specific capacitance of up to 80 μF cm^{-2}.[12] It has been further manifested that graphene intercalation enhances the electrochemical performance of MnO_2/graphene composite based supercapacitors.[13]

The recent trend of miniaturized, flexible, and wearable electronics has motivated considerable research interest in the potential of high-performance supercapacitors with large stretchability.[14−19] The pursuit of graphene-based stretchable supercapacitors can be much benefited by learning from the experience gained by carbon nanotube-based supercapacitors, which have enjoyed a longer period of study. Researchers have utilized carbon nanotube arrays, films, or fibers to fabricate stretchable supercapacitors largely through a prestraining-then-buckling strategy.[20−24] In addition to carbon nanotubes, an all-graphene core−sheath fiber based supercapacitor has been demonstrated, where the stretchability was accomplished by forming it in the shape of a spring.[25]

Furthermore, although indium tin oxide (ITO) has been the most commonly used transparent electrode, the intrinsic brittleness of ITO prevents its application where mechanical flexibility is required.[26] On the other hand, CVD-grown graphene films with high optical transparency, low sheet resistance, and desirable mechanical compliance hold high potential for transparent and stretchable electrodes.[27] It has been reported that with the same sheet resistance, graphene can show better optical transparency than ITO.[28] Therefore, the superb combination of stretchability and transparency of CVD graphene films has enabled such developments as in self-powered rolled-up displays and self-powered wearable optoelectronics.[29]

Most recently, a transparent and stretchable supercapacitor based on CVD-grown wrinkled multilayer graphene films has been reported, which is capable of sustaining a tensile strain of up to 40%.[30] An optical modulator based on a transparent CVD graphene supercapacitor was demonstrated to be compliant enough to be fabricated on flexible substrates for the potential application of electrically reconfigurable flexible coatings or smart windows.[31] Wavy-shaped PANI/graphene electrodes were also used to fabricate the stretchable supercapacitor, which showed good electrochemical performance at a maximum strain of 30%.[32]

In spite of the recent encouraging advancements summarized above, the adaptation of ultrathin CVD graphene films for stretchable and high-rate supercapacitors still remains a great challenge.

RESULTS AND DISCUSSION

In this paper, we explored the applicability of the widely used prestraining-then-buckling method[20−23,33−35] for realizing the stretchability of graphene electrodes for supercapacitors. Four-layer graphene films on an elastomeric PDMS substrate were endowed with stretchability using this approach. The multilayer graphene was processed by synthesizing individual graphene films, followed by a film transporting and laying-up process.[3] The PDMS film (around 300 μm thick) was prestretched to the tensile strain of 50%, and a four-layer graphene film was attached to the PDMS film. The graphene film spontaneously buckled upon releasing the PDMS substrate. Subsequently, the buckled graphene/PDMS laminate was rinsed by deionized water and dried at 60 °C for 12 h.

To confirm that the CVD graphene films obtained on the Cu substrate are monolayer and of high quality, the Raman spectrum of the graphene film transferred on a 300 nm thick SiO_2/Si wafer was acquired (Figure 1a). Prominent G and 2D bands were located at ~1590 and ~2689 cm^{-1}, respectively. The intensity ratio of the 2D band to the G band (I_{2D}/I_G) reached ~1.8, and the full width at half-maximum (fwhm) of a 2D band equaled 30.91 cm^{-1}, both of which provided convincing evidence of the monolayer feature of the graphene film.[8,36] Additionally, the hardly distinguishable D peak

at ~1349 cm^{-1} implied the minimal amount of defects and disorders in the graphitic material.[36]

The spectra of the four-layer buckled graphene/PDMS film at different stretching levels were also collected to evaluate the effects of tensile strain on the quality of the graphene films (Figure 1b). Note that as the Raman peaks of PDMS substrate and graphene film are obviously separated and clearly distinguishable, the contribution from the PDMS substrate to Raman feature of graphene film could be ignored.[37] Compared with monolayer graphene, the Raman spectra of four-layer buckled graphene films showed the characteristic of a much lower I_{2D}/I_G (0.52−0.81), due to the increased number of graphene layers in the laminate.[37] The weak D band at each tensile strain suggested that neither processing (the laminating and prestraining-then-buckling processes) nor stretching induced mechanical damage to the buckled graphene films. As the tensile strain increased to 40%, the G peak (~1588 cm^{-1}) showed no noticeable change, while the strain-sensitive 2D band[2] is red-shifted by 7 cm^{-1}.

Figure 2a shows the morphology of the buckled graphene layer with nanoscale, ripple-like features. The height of large ripples was around 0.6−1.5 μm (Figure 2b,c), and the height of small ripples was 50−70 nm (Figure 2d,e). The mismatch of the elastic modulus between graphene film and PDMS substrate was responsible for the buckled structure.[2] The larger graphene ripples gave rise to a bigger hollow structure, thereby providing the electrolyte with more contact area in accessing the graphene film electrodes (Figure 2b).

The proposed stretchable supercapacitor in the form of simple parallel-plate geometry (Figure 3a,b) comprised two pieces of transparent buckled graphene/PDMS films (Figure 3c), which were electrically separated by a H_2SO_4−PVA gel electrolyte. Herein, the H_2SO_4−PVA gel electrolyte, serving as both separator and electrolyte, prevented the supercapacitor from hazardous leakage and ensured the integrity of the supercapacitor.[38,39] In order to assess the transparency of the supercapacitor, optical transmittances of the assembled supercapacitor and its components were measured, as exhibited in Figure 3d. At the wavelength of 550 nm, the assembled supercapacitor based on a four-layer buckled graphene/PDMS film (82.7% transmittance) possessed an optical transmittance of 72.9%, which was much higher than that of the pioneering wrinkled graphene film based supercapacitor (48−57%)[30] and comparable to that of a highly aligned carbon nanotube sheet based supercapacitor (75%).[29] The excellent transparency of the assembled supercapacitor can be attributed to its highly transparent components of PDMS film with a transmittance of 94.6%, the electrolyte with negligible transmittance reduction, and the fact that each graphene layer gives rise to only 2.3% transmittance reduction.[40] Besides the excellent transparency, the as-received supercapacitor

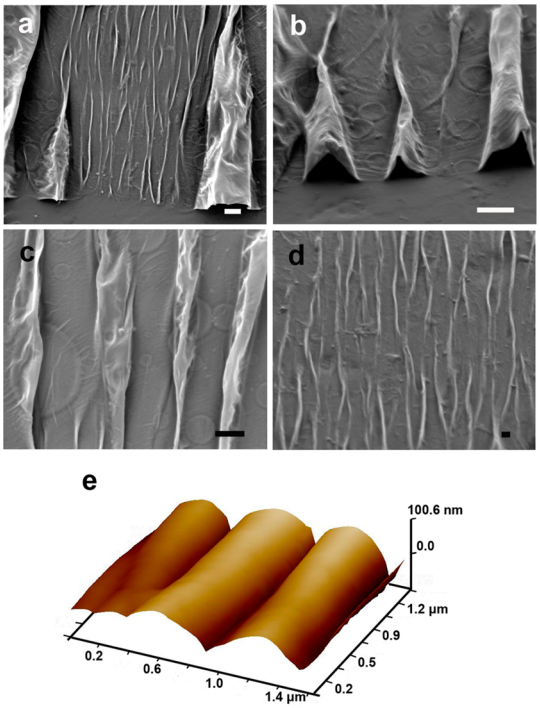

Figure 2. Morphology characterization of a four-layer buckled graphene film on PDMS substrate. (a−d) Scanning electron microscopy (SEM) images. The scale bars are 1 μm in a−c and 20 nm in d. (e) Atomic force microscopy (AFM) image of three neighboring ripples.

was also capable of withstanding tensile strains of up to 40%, as displayed in Figure 3e.

In order to investigate the dielectric and transport properties, electrochemical impedance spectroscopy (EIS) studies were conducted. Figure 4a presents the Nyquist plots at different degrees of stretching. The lines nearly vertical to the axis of the real component of impedance appeared in the low-frequency region, which demonstrated that the stretchable graphene based supercapacitor maintained an ideal capacitive behavior[41] without being affected by the stretching. The magnitude of equivalent series resistance (ESR), which determines the charge/discharge rate of the supercapacitor, can be estimated from the *x*-intercept of the Nyquist plots.[42] Specifically, increased tensile strain led to the rise of ESR from 1700 ohm to 5270 ohm, which, to some extent, had a negative effect on the rate capability.

The excellent rate capability was further analyzed by the Bode plots of imaginary specific capacitance (Figure 4b) using the serious resistor−capacitor model. The frequency corresponding to the maximum of the imaginary capacitance is the characteristic frequency of the supercapacitor, f_0, which can be used to determine the relaxation time constant (or dielectric relaxation time), $\tau_0 = 1/f_0$. The relaxation time reflects the transition between the capacitive and resistive behavior of the supercapacitor and is the minimum time required to deliver the stored energy with an efficiency

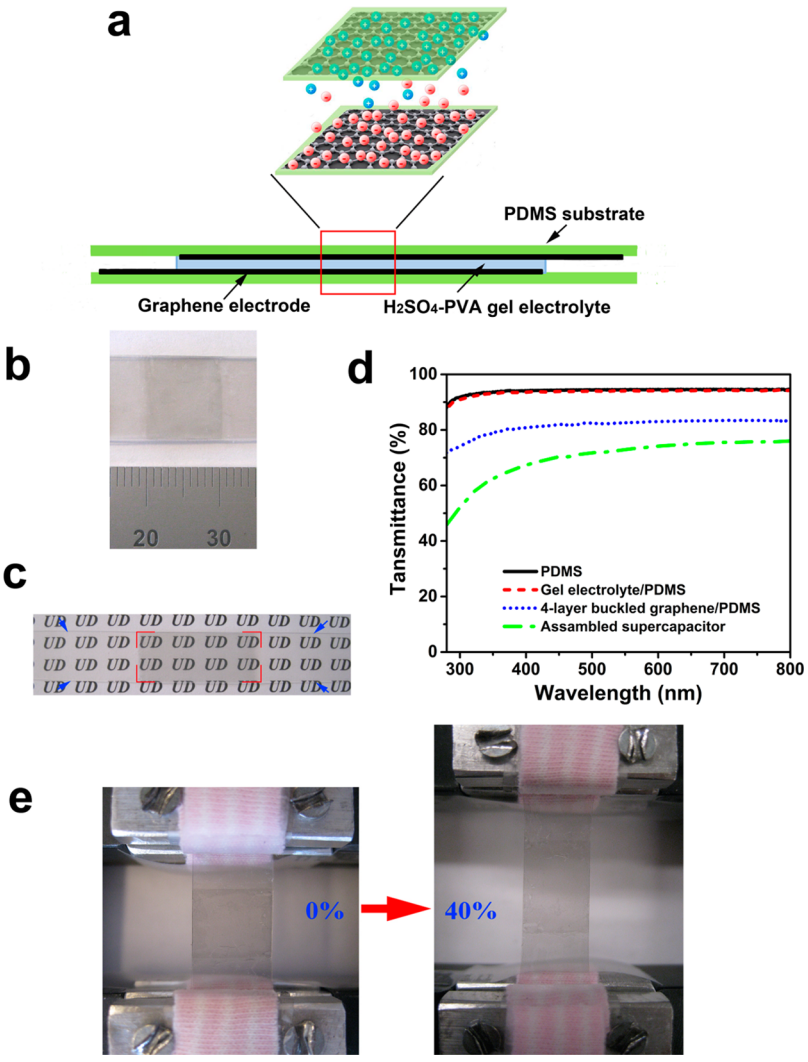

Figure 3. Optical transparency and stretchability of the graphene-based supercapacitor. (a) Schematic depiction of a transparent and stretchable supercapacitor consisting of buckled graphene/PDMS films and gel electrolyte. Digital pictures of (b) a supercapacitor based on transparent buckled graphene/PDMS films (c). (d) Transmittances of the supercapacitor and its components. (e) Digital photo of the supercapacitor stretched from the tensile strain of 0% to 40%.

of over 50%.[43−46] It is evident from Figure 4c that the frequency response slowed down from f_0 = 34.3 Hz (at a tensile strain of 0%) to f_0 = 7.92 Hz (at a tensile strain of 40%), corresponding to the time constants of 29 and 126 ms, respectively. The graphene film based supercapacitor without any stretching (at a tensile strain of 0%) possessed a very short relaxation time constant τ_0 (29 ms), which is comparable to carbon onion microsupercapacitors (26 ms), indicating the fast ion accessibility for electrosorption.[43] Although the time constant increased to 126 ms at a tensile strain of 40%, it was still comparable to or even much shorter than many carbon material based supercapacitors, for instance, 700 ms for MWCNT-based supercapacitors,[44] 700 ms for an activated carbon based microdevice,[43] 1 s for a nitrogen-doped graphene sheet electrode, and 8.3 s for a reduced graphene oxide electrode.[47] In addition, the high rate capability of supercapacitors is usually demonstrated by better capacitance retention at either high scan rates in the CV measurements or higher current densities in galvanostatic charge−discharge tests.[48]

Figure 5a and b exhibit the cyclic voltammetry (CV) curves of a supercapacitor at tensile strains of 0% and 40% in a wide range of scan rates (20−6000 mV s^{-1}). The CV curves maintained an ideal, rectangular shape at scan rates of up to 6000 mV s^{-1} at 0% and 4000 mV s^{-1} at 40%, respectively, indicating good electrical double-layer capacitive behavior and rate capability.[48] Figure 5c depicts the CV curves obtained at various tensile strains at a scan rate of 200 mV s^{-1}. The slightly enlarged areas enclosed by the CV curves at tensile strains from 0% to 40% corresponded to the enhanced area-specific capacitances of 4.27, 4.84, 5.14, and 5.33 μF cm^{-2}, which were equal to the gravimetric capacitance of 13.9, 15.7, 16.7, and 17.3 F g^{-1}, respectively. The improved electrochemical performance may be attributed to the increased pressure applied by the upper and lower PDMS films

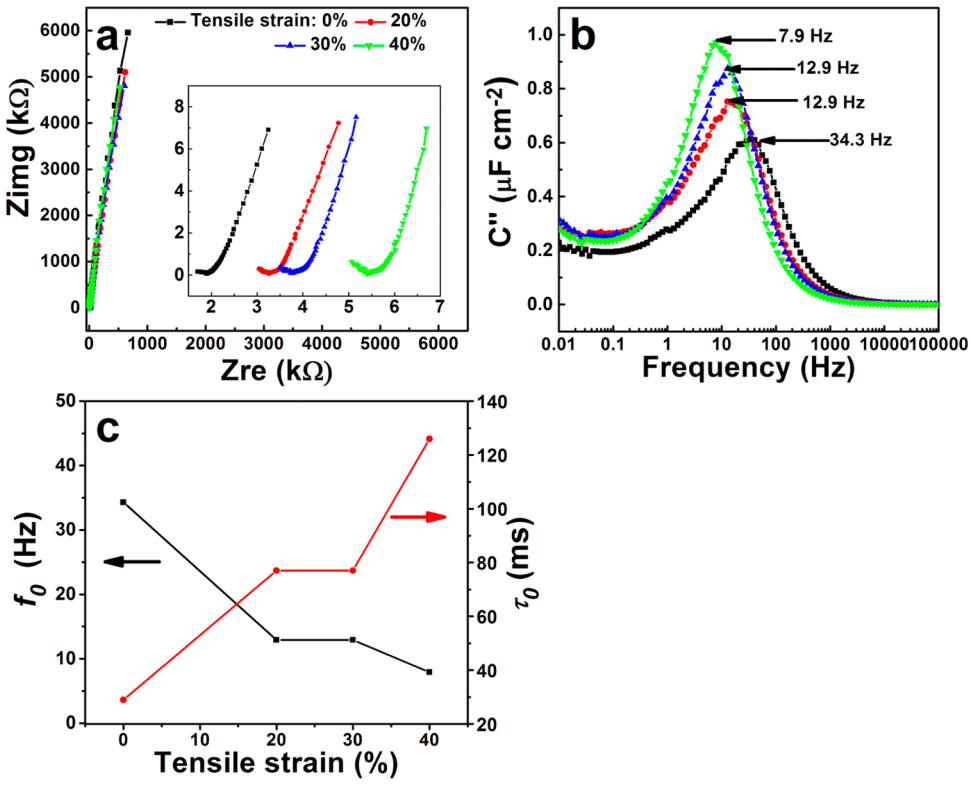

Figure 4. Kinetics properties of a buckled graphene film based supercapacitor. (a) Nyquist plots in which Zre is real impedance and Zimg is imaginary impedance. The inset is the magnification of Nyquist plots in the high-frequency region. (b) Bode plots of imaginary area specific capacitances (C''), which are calculated from EIS data. The legend for panel b is the same as for a. (c) Variations of characteristic frequency f_0 and time constant τ_0 with tensile strains of 0−40%.

during stretching by 20%, 30%, and 40%, which can facilitate the wettability of the graphene electrode.[49,50] The results achieved using only four graphene layers were comparable to those of the supercapacitor based on wrinkled graphene films with 10−20 layers.[30] At the relatively high scan rate of 4000 mV s^{-1} (Figure 5d), the slope $\Delta I/\Delta V$ (indicated by the dashed boxes) associated with ESR of the supercapacitor[39] declined gradually in the order 0% > 20% > 30% > 40%, indicating slower charge/discharge rate responses to the applied potential.[48]

As presented in Figure 5e, the specific capacitance declined with increases in scan rate. The reason for this variation was that at low scan rates the ample time facilitated full access of the ions to the electrode, while at high scan rates, the ions did not have sufficient time to access the graphene electrodes.[39] It is worth noting that when the scan rate increased by 300 times, from 20 mV s^{-1} to 6000 mV s^{-1}, the capacitance retained 67.69%, 59.12%, 63.55%, and 57.33% at the applied tensile strains of 0%, 20%, 30%, and 40%, respectively, manifesting the extraordinary rate capability of the graphene electrodes.[48] The Ragone plots in Figure 5f further confirm the excellent rate performance of the stretchable graphene film based supercapacitor. As the tensile strain changed from 0% to 40%, the average specific power and energy densities followed the trend of continuing enhancement. For the same electrolyte, the maximum specific energy densities (E_{max}) determined by specific capacitance had the highest value at the tensile strain of 40% (0.27 nWh cm^{-2}) and lowest value at 0% (0.20 nWh cm^{-2}). On the contrary, the maximum specific power density (P_{max}), being limited by ESR, had the highest value at 0% (36.48 μW cm^{-2}) and lowest value at 40% (11.77 μW cm^{-2}). Compared with the ultrathin planar CVD graphene supercapacitor (E_{max} = 2.8 nWh cm^{-2}, P_{max} = 2.0 μW cm^{-2}),[12] the stretchable supercapacitor has a much lower E_{max} but much higher P_{max} of 18 (0%) to 5 times (40%).

The superior electrochemical performance of the graphene film based supercapacitor is further demonstrated by conducting galvanostatic charge−discharge tests in the potential range 0−0.8 V at current densities from 0.45 to 2.25 μA cm^{-2} and range of stretching from 0% to 40%. Figure 6a and b show the galvanostatic charge−discharge curves at tensile strains of 0% and 40%, respectively. Here, the linear triangular time dependence of the voltage indicated sound double-layer capacitance behavior. The slightly reduced slope of the discharge curve with the increase of tensile strain in Figure 6c indicated the slight enhanced specific capacitance. At such low current densities, small *IR* drops were observed; nevertheless, the calculated ESRs were around 20 000 Ω, which was much higher than the values obtained from

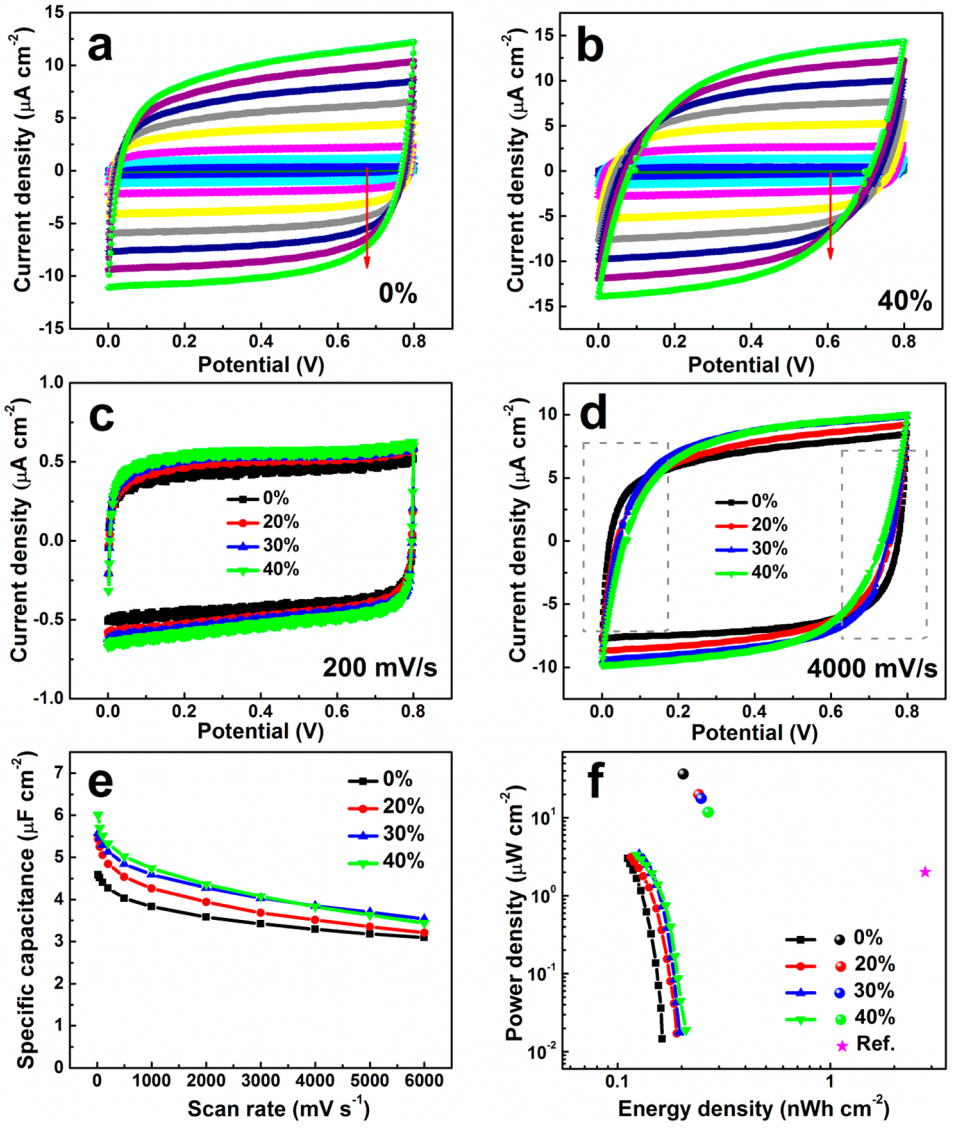

Figure 5. Electrochemical performance revealed by CV tests. (a, b) CV curves at tensile strains of 0% and 40%, respectively, at scan rates of 20, 50, 100, 200, 500, 1000, 2000, 3000, 4000, 5000, and 6000 mV s^{-1}, increasing in the arrow direction. (c, d) CV curves at scan rates of 200 and 4000 mV s^{-1}, respectively. (e) Variations of specific capacitance at different tensile strains with scan rate increasing from 20 mV s^{-1} to 6000 mV s^{-1}. (f) Ragone plots at tensile strains from 0% to 40%. The curves represent the average power and energy densities at different tensile strains, while the scattered symbols represent their maximum values. The value of "Ref." comes from an ultrathin planar graphene supercapacitor.[12]

the EIS experiments. Resulting from the extra contribution of self-discharge to the *IR* drop at a low current, especially in the circumstance of small-mass electrodes, ESR calculated on the basis of the galvanostatic charge–discharge tests may be larger than the true value.[51,52]

The electrochemical stability of the stretchable supercapacitor at a tensile strain of 40% was examined using the galvanostatic charge–discharge long-cycling method at 0.9 μA cm^{-2} for 10 000 cycles (Figure 6d). The supercapacitor possessed an excellent electrochemical stability with a capacitance retention around 100% as the cycle number increased. The capacitance retention still can achieve 98% after 10 000 cycles.

CONCLUSIONS

In conclusion, a transparent and stretchable supercapacitor based on ultrathin, buckled four-layer CVD graphene films has been reported. Fabricated through the facile prestraining-then-releasing approach in a highly controlled manner, the supercapacitor realized the unique combination of excellent stretchability (up to 40%), high optical transparency (72.9% transmittance), and outstanding electrochemical performance with extraordinary rate capability (time constant: 29–126 ms) and electrochemical stability (capacitance retention: 98% after 10 000 cycles). Overall, depending on the requirements of targeted applications, the optimal combination of these multiple

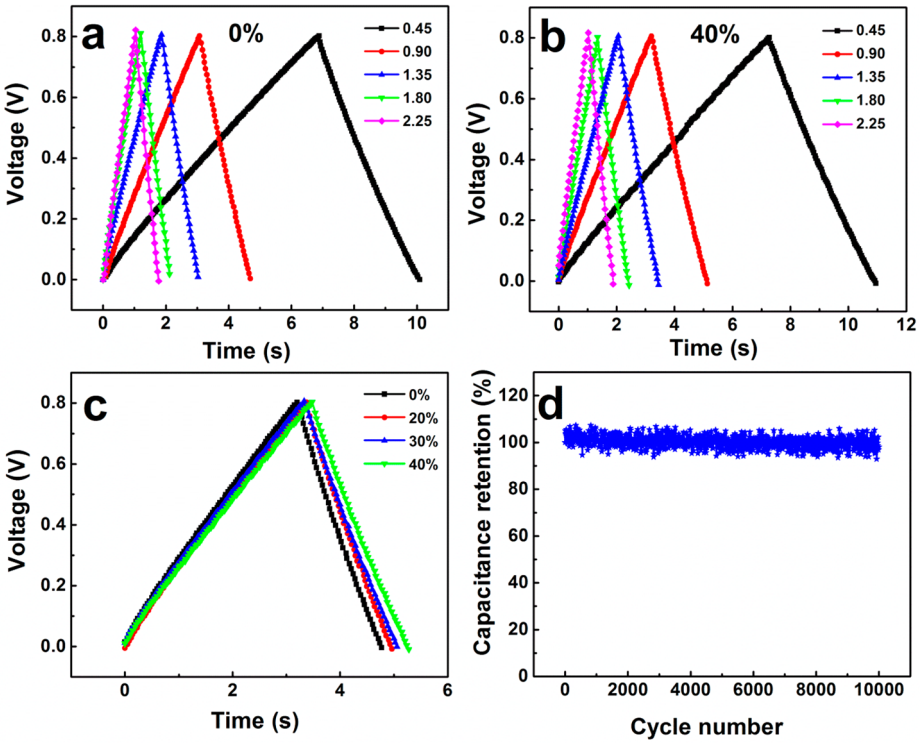

Figure 6. Galvanostatic charge–discharge measurements. (a, b) Charge–discharge curves (current densities ranging from 0.45 to 2.25 μA cm^{-2} at tensile strains of 0% and 40%, respectively). (c) Comparison of charge–discharge curves at different tensile strains. The current density is 0.9 μA cm^{-2}. (d) Capacitance retention at a tensile strain of 40% as the cycle number increased up to 10 000.

functions could be accomplished through supercapacitor design, such as modifying graphene electrodes (*e.g.*, chemical doping, increasing the layer number, or adding pseudocapacitor materials), selecting electrolytes with high operating voltage, and adopting an asymmetric design.

EXPERIMENTAL SECTION

Single-Layer Graphene Film Synthesis. The single-layer graphene films were synthesized on a Cu substrate using the CVD method. A Cu foil was annealed at 1000 °C for 1.5 h in a 2 in. quartz tube with a 2 sccm H_2 flow. Subsequently, a 20 sccm CH_4 flow was introduced for graphene growth at 30 mTorr for 0.5 h. Then, the furnace was quickly cooled to room temperature under He flow. The graphene on the back side of Cu foil was etched away by O_2 plasma.[53]

Graphene Laminating Procedure. The procedure adopted to laminate four individual graphene films into a stacked four-layer graphene film is summarized as follows. First, the single-layer graphene on Cu foil was coated by poly(methyl methacrylate) (PMMA). The Cu foil was then etched away by an aqueous solution of 0.1 M ammonium persulfate solution ($(NH_4)_2S_2O_8$). After rinsing with DI water, the floating PMMA/graphene film was scooped up by another single-layer graphene on Cu foil. The procedure was repeated three times to obtain the PMMA/four-layer graphene/copper laminate. Then, the precoated PMMA was dissolved by acetone.[54] Finally, the laminated four-layer graphene film was obtained after Cu etching and rinsing in DI water.

Raman Spectra. The Raman spectra of buckled graphene films were acquired using a WITEC CRM 200 Raman system. The excitation source is a 532 nm laser (2.33 eV) with a laser power below 0.1 mW on the buckled graphene/PDMS film to avoid laser-induced heating. The monolayer graphene film on the SiO_2/Si wafer was characterized by 514 nm (2.41 eV) Raman spectroscopy (Renishaw).

Gel Electrolyte Preparation. The H_2SO_4 gel electrolyte was prepared by mixing concentrated H_2SO_4 (6 g, 98%) with deionized water (60 mL) and then adding PVA powder (6 g, Sigma-Aldrich, M_w = 89 000–98 000). The solution was subjected to vigorous stirring throughout the mixing process and subsequent heating to 85 °C until the solution became clear.

Supercapacitor Fabrication. To fabricate a stretchable graphene-based supercapacitor, a thin layer of the liquid H_2SO_4–PVA gel electrolyte was applied on a predetermined area of the buckled graphene/PDMS film, leaving the uncoated part to be connected with current collectors. After the electrolyte solidified, two of such films were stacked together with the electrolyte-coated parts overlapping with each other. The electrical resistance between them was monitored by multimeter to avoid a short circuit. The assembled supercapacitor was placed in the fume hood under ambient conditions to allow the gel electrolyte to solidify.

Morphology Characterization. The surface morphology of the buckled four-layer graphene/PDMS film was characterized by scanning electron microscopy (Zeiss Auriga 60 FIB-SEM) and atomic force microscopy (Veeco Dimension 3100, at taping mode).

Optical Transmittances. The optical transmittances of the samples were measured by a PerkinElmer Lambda 750UV/visible/IR spectrophotometer fitted with an integrating sphere.

Electrochemical Performance Evaluation. The electrochemical performance of the supercapacitor was investigated by electrochemical impedance spectroscopy and cyclic voltammograms using a PARSTAT 2273 potentiostat/galvonostat Advanced Electrochemical System (Princeton Applied Research, USA). The galvanostatic charge–discharge cycling experiments were conducted using an Arbin potentiostat test system. EIS measurements were recorded over the frequency range of 100 kHz to10 mHz.

Conflict of Interest: The authors declare no competing financial interest.

Acknowledgment. T.-W. Chou thanks the support of the National Research Foundation of Korea through the Korean Ministry for Education, Science and Technology (MEST). The authors thank B. Wei for providing the electrochemical characterization instruments, L. Dai for helpful discussions, C. Ni and G. Zhao for assistance with microscopy observation, and R. Birkmire and P. Xin for advice on measurements of optical transmittance. P.X.'s study abroad at the University of Delaware is supported by the State Scholarship Fund of the China Scholarship Council as well as Doctorial Innovation Fund of Donghua University.

REFERENCES AND NOTES

1. Choi, H. J.; Jung, S. M.; Seo, J. M.; Chang, D. W.; Dai, L. M.; Baek, J. B. Graphene for Energy Conversion and Storage in Fuel Cells and Supercapacitors. *Nano Energy* **2012**, *1*, 534–551.
2. Wang, Y.; Yang, R.; Shi, Z.; Zhang, L.; Shi, D.; Wang, E.; Zhang, G. Super-Elastic Graphene Ripples for Flexible Strain Sensors. *ACS Nano* **2011**, *5*, 3645–3650.
3. Bae, S.; Kim, H.; Lee, Y.; Xu, X.; Park, J.-S.; Zheng, Y.; Balakrishnan, J.; Lei, T.; Ri Kim, H.; Song, Y. I.; *et al*. Roll-to-Roll Production of 30-Inch Graphene Films for Transparent Electrodes. *Nat. Nanotechnol.* **2010**, *5*, 574–578.
4. Kim, K. S.; Zhao, Y.; Jang, H.; Lee, S. Y.; Kim, J. M.; Kim, K. S.; Ahn, J.-H.; Kim, P.; Choi, J.-Y.; Hong, B. H. Large-Scale Pattern Growth of Graphene Films for Stretchable Transparent Electrodes. *Nature* **2009**, *457*, 706–710.
5. Huang, Y.; Liang, J.; Chen, Y. An Overview of the Applications of Graphene-Based Materials in Supercapacitors. *Small* **2012**, *8*, 1805–1834.
6. Sun, Y.; Wu, Q.; Shi, G. Graphene Based New Energy Materials. *Energy Environ. Sci.* **2011**, *4*, 1113–1132.
7. Kang, J.; Shin, D.; Bae, S.; Hong, B. H. Graphene Transfer: Key for Applications. *Nanoscale* **2012**, *4*, 5527–5537.
8. Li, X.; Cai, W.; An, J.; Kim, S.; Nah, J.; Yang, D.; Piner, R.; Velamakanni, A.; Jung, I.; Tutuc, E.; *et al*. Large-Area Synthesis of High-Quality and Uniform Graphene Films on Copper Foils. *Science* **2009**, *324*, 1312–1314.
9. Mattevi, C.; Kim, H.; Chhowalla, M. A Review of Chemical Vapour Deposition of Graphene on Copper. *J. Mater. Chem.* **2011**, *21*, 3324–3334.
10. Miller, J. R.; Outlaw, R. A.; Holloway, B. C. Graphene Double-Layer Capacitor with ac Line-Filtering Performance. *Science* **2010**, *329*, 1637–1639.
11. Miller, J. R.; Outlow, R. A.; Holloway, B. C. Graphene Electric Double Layer Capacitor with Ultra-High-Power Performance. *Electrochim. Acta* **2011**, *56*, 10443–10449.
12. Yoo, J. J.; Balakrishnan, K.; Huang, J.; Meunier, V.; Sumpter, B. G.; Srivastava, A.; Conway, M.; Mohana Reddy, A. L.; Yu, J.; Vajtai, R.; *et al*. Ultrathin Planar Graphene Supercapacitors. *Nano Lett.* **2011**, *11*, 1423–1427.
13. Lee, H.; Kang, J.; Cho, M. S.; Choi, J.-B.; Lee, Y. MnO_2/Graphene Composite Electrodes for Supercapacitors: the Effect of Graphene Intercalation on Capacitance. *J. Mater. Chem.* **2011**, *21*, 18215–18219.
14. Jost, K.; Stenger, D.; Perez, C. R.; McDonough, J. K.; Lian, K.; Gogotsi, Y.; Dion, G. Knitted and Screen Printed Carbon-Fiber Supercapacitors for Applications in Wearable Electronics. *Energy Environ. Sci.* **2013**, *6*, 2698–2705.
15. Hu, L.; Pasta, M.; Mantia, F. L.; Cui, L.; Jeong, S.; Deshazer, H. D.; Choi, J. W.; Han, S. M.; Cui, Y. Stretchable, Porous, and Conductive Energy Textiles. *Nano Lett.* **2010**, *10*, 708–714.
16. Jost, K.; Perez, C. R.; McDonough, J. K.; Presser, V.; Heon, M.; Dion, G.; Gogotsi, Y. Carbon Coated Textiles for Flexible Energy Storage. *Energy Environ. Sci.* **2011**, *4*, 5060–5067.
17. Jost, K.; Dion, G.; Gogotsi, Y. Textile Energy Storage in Perspective. *J. Mater. Chem. A* **2014**, *2*, 10776–10787.
18. Beidaghi, M.; Gogosti, Y. Capacitive Energy Storage in Micro-Scale Devices: Recent Advances in Design and Fabrication of Micro-supercapacitors. *Energy Environ. Sci.* **2014**, *7*, 867–884.
19. Xie, K.; Wei, B. Materials and Structures for Stretchable Energy Storage and Conversion Devices. *Adv. Mater.* **2014**, *26*, 3592–3617.
20. Yu, C.; Masarapu, C.; Rong, J.; Wei, B.; Jiang, H. Stretchable Supercapacitors Based on Buckled Single-Walled Carbon-Nanotube Macrofilms. *Adv. Mater.* **2009**, *21*, 4793–4797.
21. Li, X.; Gu, T.; Wei, B. Dynamic and Galvanic Stability of Stretchable Supercapacitors. *Nano Lett.* **2012**, *12*, 6366–6371.
22. Niu, Z.; Dong, H.; Zhu, B.; Li, J.; Hng, H. H.; Zhou, W.; Chen, X.; Xie, S. Highly Stretchable, Integrated Supercapacitors Based on Single-Walled Carbon Nanotube Films with Continuous Reticulate Architecture. *Adv. Mater.* **2013**, *25*, 1058–1064.
23. Xu, P.; Gu, T.; Cao, Z.; Wei, B.; Yu, J.; Li, F.; Byun, J.-H.; Lu, W.; Li, Q.; Chou, T.-W. Carbon Nanotube Fiber Based Stretchable Wire-Shaped Supercapacitors. *Adv. Energy Mater.* **2014**, *4*, 1300759.
24. Yang, Z.; Deng, J.; Chen, X.; Ren, J.; Peng, H. A Highly Stretchable, Fiber-Shaped Supercapacitor. *Angew. Chem., Int. Ed.* **2013**, *52*, 13453–13457.
25. Meng, Y.; Zhao, Y.; Hu, C.; Cheng, H.; Hu, Y.; Zhang, Z.; Shi, G.; Qu, L. All-Graphene Core-Sheath Microfibers for All-Solid-State, Stretchable Fibriform Supercapacitors and Wearable Electronic Textiles. *Adv. Mater.* **2013**, *25*, 2326–2331.
26. Gomez De Arco, L.; Zhang, Y.; Schlenker, C. W.; Ryu, K.; Thompson, M. E.; Zhou, C. Continuous, Highly Flexible, and Transparent Graphene Films by Chemical Vapor Deposition for Organic Photovoltaics. *ACS Nano* **2010**, *4*, 2865–2873.
27. Wan, X.; Huang, Y.; Chen, Y. Focusing on Energy and Optoelectronic Applications: A Journey for Graphene and Graphene Oxide at Large Scale. *Acc. Chem. Res.* **2012**, *45*, 598–607.
28. Bonaccorso, F.; Sun, Z.; Hasan, T.; Ferrari, A. C. Graphene Photonics and Optoelectronics. *Nat. Photonics* **2010**, *4*, 611–622.
29. Chen, T.; Peng, H.; Durstock, M.; Dai, L. High-Performance Transparent and Stretchable All-Solid Supercapacitors Based on Highly Aligned Carbon Nanotube Sheets. *Sci. Rep.* **2014**, *4*, 03612.
30. Chen, T.; Xue, Y.; Roy, A. K.; Dai, L. Transparent and Stretchable High-Performance Supercapacitors Based on Wrinkled Graphene Electrodes. *ACS Nano* **2013**, *8*, 1039–1046.
31. Polat, E. O.; Kocabas, C. Broadband Optical Modulators Based on Graphene Supercapacitors. *Nano Lett.* **2013**, *13*, 5851–5857.
32. Xie, Y.; Liu, Y.; Zhao, Y.; Tsang, Y. H.; Lau, S. P.; Huang, H.; Chai, Y. Stretchable All-Solid-State Supercapacitor with Wavy Shaped Polyaniline/Graphene Electrode. *J. Mater. Chem. A* **2014**, *2*, 9142–9149.
33. Khang, D.-Y.; Xiao, J.; Kocabas, C.; MacLaren, S.; Banks, T.; Jiang, H.; Huang, Y. Y.; Rogers, J. A. Molecular Scale Buckling Mechanics in Individual Aligned Single-Wall Carbon Nanotubes on Elastomeric Substrates. *Nano Lett.* **2008**, *8*, 124–130.
34. Xu, F.; Wang, X.; Zhu, Y.; Zhu, Y. Wavy Ribbons of Carbon Nanotubes for Stretchable Conductors. *Adv. Funct. Mater.* **2012**, *22*, 1279–1283.
35. Zang, J.; Ryu, S.; Pugno, N.; Wang, Q.; Tu, Q.; Buehler, M. J.; Zhao, X. Multifunctionality and Control of the Crumpling and Unfolding of Large-Area Graphene. *Nat. Mater.* **2013**, *12*, 321–325.
36. Graf, D.; Molitor, F.; Ensslin, K.; Stampfer, C.; Jungen, A.; Hierold, C.; Wirtz, L. Spatially Resolved Raman Spectroscopy of Single- and Few-Layer Graphene. *Nano Lett.* **2007**, *7*, 238–242.
37. Wang, Y. Y.; Ni, Z. H.; Yu, T.; Shen, Z. X.; Wang, H. M.; Wu, Y. H.; Chen, W.; Shen Wee, A. T. Raman Studies of Monolayer Graphene: The Substrate Effect. *J. Phys. Chem. C* **2008**, *112*, 10637–10640.

38. Wu, Z. S.; Parvez, K.; Feng, X. L.; Mullen, K. Graphene-Based in-Plane Micro-Supercapacitors With High Power and Energy Densities. *Nat. Commun.* **2013**, *4*, 2487.
39. Niu, Z.; Zhang, L.; Liu, L.; Zhu, B.; Dong, H.; Chen, X. All-Solid-State Flexible Ultrathin Micro-Supercapacitors Based on Graphene. *Adv. Mater.* **2013**, *25*, 4035–4042.
40. Nair, R. R.; Blake, P.; Grigorenko, A. N.; Novoselov, K. S.; Booth, T. J.; Stauber, T.; Peres, N. M. R.; Geim, A. K. Fine Structure Constant Defines Visual Transparency of Graphene. *Science* **2008**, *320*, 1308.
41. Conway, B. E. *Electrochemical Supercapacitors: Scientific Fundamentals and Technological Applications*; Kuwer Academic/Plenum Press: New York, 1999; pp 528−529.
42. Yang, X.; Zhu, J.; Qiu, L.; Li, D. Bioinspired Effective Prevention of Restacking in Multilayered Graphene Films: Towards the Next Generation of High-Performance Supercapacitors. *Adv. Mater.* **2011**, *23*, 2833–2838.
43. Pech, D.; Brunet, M.; Durou, H.; Huang, P. H.; Mochalin, V.; Gogotsi, Y.; Taberna, P. L.; Simon, P. Ultrahigh-Power Micrometre-Sized Supercapacitors Based on Onion-Like Carbon. *Nat. Nanotechnol.* **2010**, *5*, 651–654.
44. Portet, C.; Yushin, G.; Gogotsi, Y. Electrochemical Performance of Carbon Onions, Nanodiamonds, Carbon Black and Multiwalled Nanotubes in Electrical Double Layer Capacitors. *Carbon* **2007**, *45*, 2511–2518.
45. Taberna, P. L.; Simon, P.; Fauvarque, J. F. Electrochemical Characteristics and Impedance Spectroscopy Studies of Carbon-Carbon Supercapacitors. *J. Electrochem. Soc.* **2003**, *150*, A292–A300.
46. Zhang, J.; Zhao, X. S. On the Configuration of Supercapacitors for Maximizing Electrochemical Performance. *ChemSusChem* **2012**, *5*, 818–841.
47. Wang, D. W.; Min, Y. G.; Yu, Y. H.; Peng, B. A General Approach for Fabrication of Nitrogen-Doped Graphene Sheets and Its Application in Supercapacitors. *J. Colloid Interface Sci.* **2014**, *417*, 270–277.
48. Bo, Z.; Zhu, W.; Ma, W.; Wen, Z.; Shuai, X.; Chen, J.; Yan, J.; Wang, Z.; Cen, K.; Feng, X. Vertically Oriented Graphene Bridging Active-Layer/Current-Collector Interface for Ultrahigh Rate Supercapacitors. *Adv. Mater.* **2013**, *25*, 5799–5806.
49. Li, X.; Rong, J.; Wei, B. Electrochemical Behavior of Single-Walled Carbon Nanotube Supercapacitors under Compressive Stress. *ACS Nano* **2010**, *4*, 6039–6049.
50. Masarapu, C.; Wang, L.-P.; Li, X.; Wei, B. Tailoring Electrode/Electrolyte Interfacial Properties in Flexible Supercapacitors by Applying Pressure. *Adv. Energy Mater.* **2012**, *2*, 546–552.
51. Wang, X.; Zhang, Y.; Zhi, C.; Wang, X.; Tang, D.; Xu, Y.; Weng, Q.; Jiang, X.; Mitome, M.; Golberg, D.; *et al*. Three-Dimensional Strutted Graphene Grown by Substrate-Free Sugar Blowing for High-Power-Density Supercapacitors. *Nat. Commun.* **2013**, *4*, 2905.
52. Stoller, M. D.; Ruoff, R. S. Best Practice Methods for Determining an Electrode Material's Performance for Ultracapacitors. *Energy Environ. Sci.* **2010**, *3*, 1294–1301.
53. Kang, J.; Hwang, S.; Kim, J. H.; Kim, M. H.; Ryu, J.; Seo, S. J.; Hong, B. H.; Kim, M. K.; Choi, J.-B. Efficient Transfer of Large-Area Graphene Films onto Rigid Substrates by Hot Pressing. *ACS Nano* **2012**, *6*, 5360–5365.
54. Li, X.; Zhu, Y.; Cai, W.; Borysiak, M.; Han, B.; Chen, D.; Piner, R. D.; Colombo, L.; Ruoff, R. S. Transfer of Large-Area Graphene Films for High-Performance Transparent Conductive Electrodes. *Nano Lett.* **2009**, *9*, 4359–4363.